

Cross-sectional scanning tunneling microscopy of Mn-doped GaAs: Theory and experiment

J. M. Sullivan,* G. I. Boishin,[†] L. J. Whitman, A. T. Hanbicki, B. T. Jonker, and S. C. Erwin
Naval Research Laboratory, Washington, D.C. 20375, USA
 (Received 7 July 2003; published 23 December 2003)

We report first-principles calculations of the energetics and simulated scanning tunneling microscopy (STM) images for Mn dopants near the GaAs (110) surface, and compare the results with cross-sectional STM images. The Mn configurations considered here include substitutionals, interstitials, and complexes of substitutionals and interstitials in the first three layers near the surface. Based on detailed comparisons of the simulated and experimental images, we identify three types of Mn configurations imaged at the surface: (1) single Mn substitutionals, (2) pairs of Mn substitutionals, and (3) complexes of Mn substitutionals and interstitials.

DOI: 10.1103/PhysRevB.68.235324

PACS number(s): 68.37.Ef, 75.50.Pp, 71.55.Eq

I. INTRODUCTION

GaAs can be doped with Mn to form a dilute magnetic semiconductor with a Curie temperature as high as 160 K.¹⁻³ It is generally accepted that holes created by the substitution of Mn for Ga mediate the ferromagnetic interaction between Mn dopants in this material.^{4,5} Naively, each substitutional Mn is expected to produce one hole; therefore the nominal hole concentration, p , should be equal to the Mn concentration. For typical Mn fractions of 5%, this implies a hole concentration $p = 1.1 \times 10^{21} \text{ cm}^{-3}$. Measured hole concentrations of as-grown material are much less than this, typically by a factor of ~ 3 . The source of this compensation remains somewhat controversial, having been variously attributed to either excess As in the form of antisites and interstitials⁶⁻⁹ or Mn interstitials.¹⁰⁻¹³ Recent experiments show that careful annealing near the growth temperature can significantly enhance the conductivity and hole concentration.^{3,11} This, as well as recent ion channelling experiments,¹¹ suggests that interstitial Mn is the more likely source. A complete picture is lacking, however; for example, the distribution of Mn interstitials in as-grown material is still unclear.

Cross-sectional scanning tunneling microscopy (XSTM) is an effective tool for addressing this issue because it can image, with atomic resolution, the structural and electronic configuration of impurities and defects as they are present in the bulk. There are several recent XSTM studies of Mn-doped GaAs;¹³⁻¹⁶ these studies used the correlation between transport data, level of Mn doping, and observed defect density to infer the location (substitutional versus interstitial) of Mn dopants and As antisites. The relative abundance of As antisites and interstitial Mn deduced by these studies lacks a clear consensus: one study finds that antisites are not present at all,¹⁵ while another finds that both antisites and interstitial Mn are present, and compensate substitutional Mn.¹³

To investigate the nature of dopants and defects in this material, we performed high-resolution XSTM measurements on a (110) cleavage plane of Mn-doped GaAs and used first-principles calculations to interpret the images. Specifically, we used density-functional theory to simulate STM images for a number of Mn configurations near the GaAs (110) surface. Configurations were chosen based on their calculated energetic stability, and included several metastable

configurations that would probably be kinetically stabilized. A detailed comparison of the resulting simulated and experimental images leads us to the following conclusions: (1) isolated substitutional Mn as well as pairs of substitutional Mn occur with roughly comparable frequency in bulk Mn-doped GaAs and (2) interstitial Mn is typically bound in complexes with substitutional Mn in several different configurations.

II. EXPERIMENTAL XSTM IMAGES

The Mn-doped GaAs sample used in this study was grown by molecular-beam epitaxy (MBE) using well established methods and conditions.¹⁷ A buffer layer of high quality undoped GaAs was first grown on an n -type GaAs substrate. This was followed by growth of a 100-nm-thick GaAs buffer layer grown at 250 °C and a 260-nm-thick layer of Mn-doped GaAs at the same temperature. Growth quality was monitored by reflection high-energy electron diffraction. The Mn concentration was determined with x-ray diffraction to be $\sim 1\%$.

This sample was then characterized by XSTM measurements in a multichamber ultrahigh-vacuum facility. In order to obtain an atomically abrupt cleave across the epilayer, the samples were thinned *ex situ* to $\leq 200 \mu\text{m}$. After being loaded into the XSTM chamber (base pressure $\leq 10^{-10}$ Torr), the samples were scribed and cleaved *in situ* to expose a (110) surface (perpendicular to the MBE growth direction), as previously described.¹⁸ The constant-current (40 pA) images shown here are of filled electronic states measured with a sample bias of -2.5 V .

Figure 1 shows the results of filled-state XSTM measurements on this sample. The scan area of this image is $170 \times 170 \text{ \AA}^2$ and displays ~ 1500 surface atoms. Filled-state STM images of GaAs (110) reveal the As surface sublattice; the Ga sublattice evident in empty-state images, on the other hand, is not directly revealed in this image. Since only the top As atoms contribute, STM of the GaAs (110) surface reveals only every other layer in the (001) direction.

Figure 1 reveals many surface features not normally seen in STM of the GaAs (110) surface. Several occur with enough regularity to warrant close attention. Feature A is an elliptical region of intensity in an As (001) plane with major and minor axes the size of two and one As surface atoms, respectively. Feature B is circular, and only slightly larger

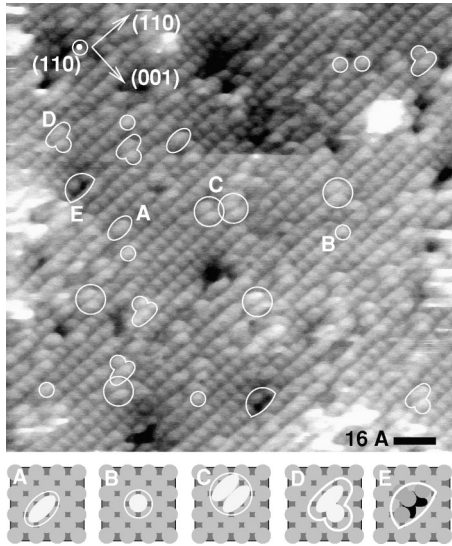


FIG. 1. Constant-current filled-state XSTM image of a (110) cleavage plane of Mn-doped GaAs (001). Five reproducible features (A–E) are marked on the image and drawn schematically below.

and more intense than the contributions from the surrounding As. Feature C is more diffuse and broad than both A and B, with intensity spread over two pairs of As atoms in neighboring (001) planes. As discussed in more detail below, this is what one would expect if there were two A features in neighboring As (001) planes. Feature D is of similar shape to that of C but is more asymmetric, with one side of the defect the size of a single surface As atom. There does not appear to be a preferred crystalline orientation of feature D, as different orientations are visible in Fig. 1. Feature E is a dark region close to a surface As atom displaced in the $(00\bar{1})$ direction; there is also an overall apparent depression in the vicinity of this feature, characteristic of band bending that occurs near positively charged defects on a p -type surface.¹⁹

On the basis of the experimental data alone it is extremely difficult, if not impossible, to determine what dopants or defects produce these features. As we show in this work, however, when interpreted with first-principles theory, these measurements resolve both the type and geometric configuration of Mn dopants in GaAs.

III. THEORETICAL APPROACH

A. Physical and electronic structure

We modeled the GaAs (110) surface in a supercell slab geometry consisting of five layers of GaAs in a 4×4 surface unit cell. A vacuum region of 13.4 \AA was used for all the calculations. In such a cell the separation between a dopant and its periodic image is $\sim 16 \text{ \AA}$, sufficiently large to ensure that dopants interact only negligibly with their periodic images. The bottom layer of the slab was passivated; the atomic positions were fully relaxed in all but the bottom two layers.

The wave functions and charge density were expanded in a plane-wave basis and evaluated using an ultrasoft pseudopotential approach^{20,21} as implemented in the VASP code.^{22–24}

Electron correlations were treated at the level of the local spin-density approximation with total energies converged to 10^{-4} eV .

A single wave vector was used to sample the Brillouin zone of the slab supercells and a plane-wave cutoff of 227.24 eV was used for all the calculations. For supercells containing Mn, atoms within $\sim 7.0 \text{ \AA}$ of the Mn site(s) were fully relaxed until the total energy between two structural configurations changed by less than 10^{-3} eV .

B. Simulated STM images

Theoretical STM images were simulated using the method of Tersoff and Hamann.²⁵ In this approach, the central quantity is the local density of states (LDOS) near the surface. The LDOS is integrated over an energy range determined by the experimental bias voltage; contours of constant energy-integrated LDOS simulate a constant-current image. For filled state imaging, the upper bound of this energy range is the Fermi level. The Mn-doped GaAs sample under consideration in this work is p type with an estimated hole density of 10^{19} cm^{-3} , so that the Fermi level should be near the valence-band maximum (VBM). Since we do not know the distribution of donors and acceptors present in the sample, this information alone is not sufficient to determine the exact location of the Fermi level for our sample. However, we have found that, as a consequence of the large bias, the simulated images are rather insensitive to the value of the Fermi level used in the LDOS integration, and so we choose arbitrarily a point 0.4 eV above the VBM as the upper bound for all the STM simulations. For this choice, the Fermi level is above the acceptor level of substitutional Mn and below the donor levels of interstitial Mn. Simulations performed with the position of the Fermi level shifted by $\pm 0.3 \text{ eV}$ give similar results. The location of the VBM for each type of dopant was determined by inspection of the total DOS relative to that projected onto the dopant site.

As a measure of the agreement between simulated and measured STM images, we consider mainly the overall shape and spatial extent of features of interest. The defect-free (110) surface has a $(\bar{1}10)$ mirror-plane symmetry, so it is also useful to note whether a particular dopant configuration preserves, even approximately, this symmetry. Finally, we use qualitative arguments to judge whether the number of observed features are consistent with our total-energy calculations.

IV. SUBSTITUTIONAL Mn

A. Simple substitutional dopants

Substitutional Mn dopants are of primary importance for the magnetic and transport properties of Mn-doped GaAs, and hence we discuss the simulated STM images for these types of dopants first. Since STM is a near-surface sensitive probe, we have only considered substitutional Mn dopants in the top three layers near the (110) surface, as shown in Fig. 2(a).

We will use the notation $s(n)$ to denote a substitutional Mn in layer n (with the topmost surface layer defined as n

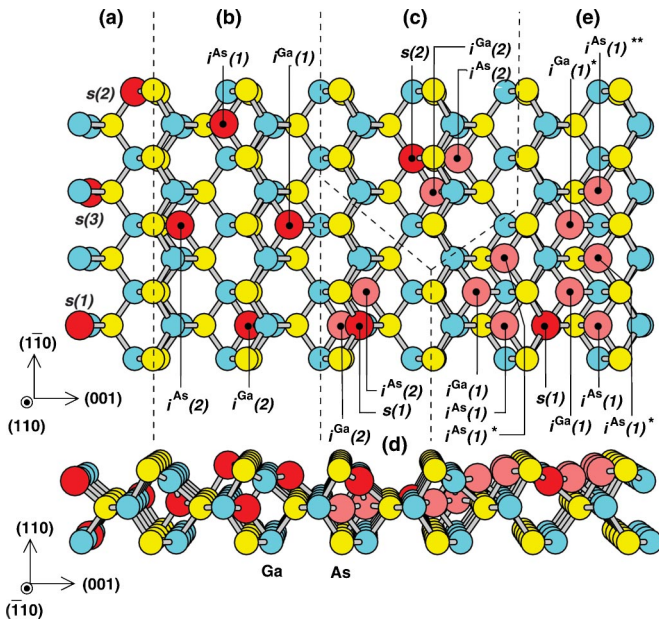


FIG. 2. (Color online) Top view (upper) and side view (lower) showing the Mn dopant configurations considered in this work. Ga, As, and Mn atoms are shown as cyan, yellow, and red circles, respectively. The dashed lines separate regions containing different types of dopants. From left to right: (a) substitutional Mn in the first three layers, (b) interstitial Mn in the first two layers, (c) complexes of substitutional and interstitial Mn in layer 2, (d) complexes of substitutional Mn in layer 1 and interstitial Mn in layer 2, (e) complexes of substitutional and interstitial Mn both in layer 1. For the complexes in regions (c), (d), and (e), several alternative locations of the interstitial Mn involved in the complex are shown in a lighter shade of red. See text for explanation of the notation.

=1). Figures 3(a), 3(b), and 3(c) show the simulated images from $s(1)$, $s(2)$, and $s(3)$, respectively. The $s(1)$ and $s(3)$ images are strikingly similar, for the following reasons. $s(1)$ forms bonds with two As atoms that are nominally in the same plane; likewise for the $s(3)$ Mn atom. Thus the overall shape of the dopant image consists of three overlapping maxima, centered on the two As atoms and on the Mn atom, giving rise to an elongated feature with a $(\bar{1}10)$ mirror-plane symmetry. Hence, both of these sites are consistent with feature A in Fig. 1.

$s(2)$ on the other hand, has a very different image. $s(2)$ forms a bond with an As atom in the top layer, with the bond pointing toward the surface. The perturbation due to $s(2)$ is centered on the surface As site involved in the bond. This overlaps with the contribution from the Mn dopant itself, and so the shape is more circular compared to $s(1)$ and $s(3)$. Thus it enhances a single As site and has a $(\bar{1}10)$ mirror-plane symmetry. These agree qualitatively with the characteristics of feature B in Fig. 1, leading us to identify those features as arising from $s(2)$ dopants.

B. Substitutional Mn pairs

Since there will always be some fraction of neighboring Mn that occur simply by chance, we consider pairs of substitutional Mn as well. Figures 3(d), 3(e), and 3(f) show

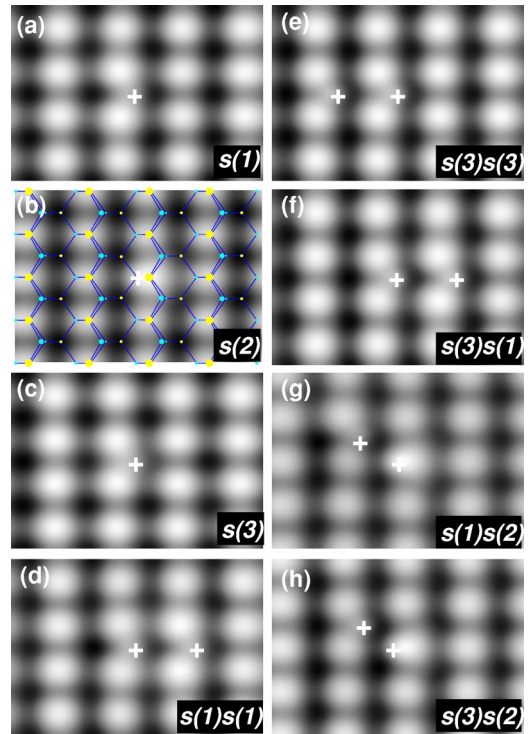


FIG. 3. Panels (a), (b), and (c) show simulated STM images of isolated Mn substitutionals. Panels (d) through (h) show simulated images for Mn substitutional pairs. Mn positions are marked with +. The crystalline orientation is the same as in Fig. 2.

simulated images of pairs of Mn substitutionals $s(1)s(1)$, $s(3)s(3)$, and $s(3)s(1)$, respectively. For the $s(3)s(1)$ pair, we note that even though the two Mn involved are ~ 6.8 Å apart, and in different atomic planes, because of the projected view of the STM scan the appearance of this pair is quite similar to those of the $s(1)s(1)$ and $s(3)s(3)$ pairs. All three of these simulated images have a shape comparable to that of feature C in Fig. 1. Common aspects include a region of low intensity between the two dopants, a $(\bar{1}10)$ mirror-plane symmetry (the experimental data only approximately have this symmetry) and a similar spatial extent involving four surface As atoms. It is also interesting to note that these pairs have simulated images that are essentially a linear superposition of the images of the isolated substitutionals shown in Figs. 3(a) and 3(c). This suggests that, at the level of detail that STM reveals, two substitutional Mn do not interact very strongly when they are next-nearest neighbors.

Figures 3(g) and 3(h) show the simulated images for nearest-neighbor substitutional pairs $s(1)s(2)$ and $s(3)s(2)$, respectively. Overall, the simulated images of these pairs are similar to what one would obtain from a linear superposition of the images of the isolated defects. However, the simulated image for $s(1)s(2)$ clearly reveals that the contribution from the $s(1)$ dopant is now asymmetric, lacking a $(\bar{1}10)$ mirror plane. This indicates that substitutional pairs interact more strongly when they are in nearest-neighbor configuration than in the next-nearest-neighbor configuration described in the paragraph above. The shape of these simulated images is generally consistent with that of feature D in Fig. 1, with a

characteristic “L” shape involving three As atoms, two of which are in the same As (001) plane. We have not found any other dopants that yield such a favorable comparison to the experimental data, leading us to identify feature D as $s(1)s(2)$ and $s(3)s(2)$ pairs. In the experimental data one can observe three of the four possible crystal orientations of these pairs of substitutionals.

An estimate of the number of neighboring pairs of Mn substitutionals based on a random distribution of Mn on the Ga sublattice is much lower than the number of compound features, in particular those labeled “C,” seen in Fig. 1. One possible explanation is positional correlation among the substitutional dopants as suggested by the strong short-range attraction between substitutional Mn found in a recent theoretical study.²⁶ Moreover, such clusters have recently been invoked in Monte Carlo calculations to investigate the phase diagram of Mn-doped GaAs with quantitative estimates of the ferromagnetic ordering temperature in agreement with experiment.^{27,28} Nevertheless, it is unlikely that a description based entirely on substitutionals and clusters of substitutionals can describe the frequency and shapes of all the features in Fig. 1. This suggests that other Mn complexes, in particular those involving interstitial Mn, may help explain the remaining features.

V. DOPANT COMPLEXES

A. Total-energy considerations

It has recently been shown that although the formation energy of interstitial Mn is much higher than that of substitutional Mn in bulk GaAs, the presence of the (001) growth surface significantly enhances the likelihood of Mn occupying interstitial sites.¹² Thus one expects that both substitutional and interstitial Mn will be present in typical Mn-doped GaAs samples, as shown by recent measurements of the Mn distribution in Mn-doped GaAs.¹¹ That both are relevant to the observed magnetic and transport properties of Mn-doped GaAs has been addressed in recent theoretical studies of the magnetic interaction in nearest-neighbor pairs of substitutional and interstitial Mn,²⁹ and in complexes composed of an interstitial Mn trapped between two neighboring substitutionals.³⁰ In the bulk, the barrier for diffusion of a charged ($+2e$) interstitial Mn is ~ 0.5 eV; therefore at room temperature we expect interstitial Mn to rapidly diffuse throughout the bulk material unless it becomes kinetically trapped. Since substitutional dopants are acceptors, they are a natural trap for interstitials, electrostatically binding to them in a number of different physical configurations. Clustering phenomena for compensating dopants such as these have recently been predicted using Monte Carlo techniques.³¹ On the other hand, since interstitial Mn in bulk is a double donor with charge of $+2e$, under conditions of filled-state imaging (for which the tip is positively biased relative to the sample) free interstitial Mn will be repelled away from the surface, leaving behind only those interstitials that are bound in complexes. To determine which such interstitial-substitutional complexes are most likely to be present, we turn to total-energy calculations.

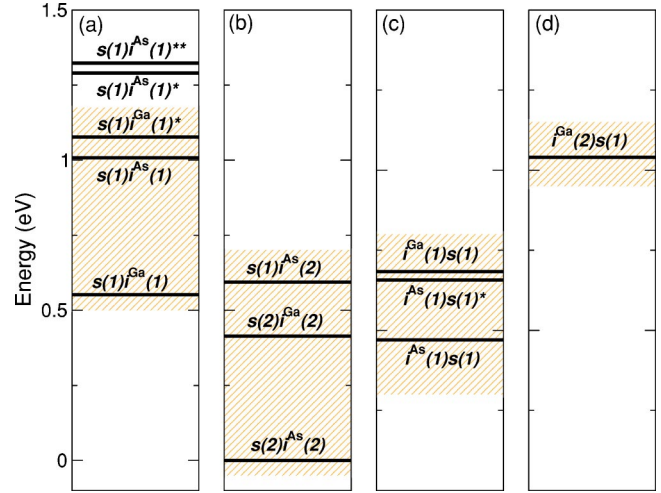


FIG. 4. Relative total energies of complexes of interstitial and substitutional Mn near the GaAs (110) surface: (a) $s(1)i^{\text{Ga}}(1)$ and $s(1)i^{\text{As}}(1)$, (b) $s(m)i^{\text{Ga}}(2)$ and $s(m)i^{\text{As}}(2)$ ($m=1,2$), (c) $i^{\text{Ga}}(1)s(1)$ and $i^{\text{As}}(1)s(1)$, and (d) $i^{\text{Ga}}(2)s(1)$. Simulated STM images are provided for the low-energy configurations in the shaded regions.

To simplify the discussion, we extend the notation introduced earlier to now include Mn interstitials, and complexes of interstitial and substitutional Mn. Isolated interstitial Mn in layer n , coordinated to As and Ga, will be referred to as $i^{\text{As}}(n)$ and $i^{\text{Ga}}(n)$, respectively. For reference, the configuration of isolated interstitial dopants in the first two layers is shown in Fig. 2(b). Complexes composed of interstitial and substitutional Mn will be referred to with a composite notation that takes into account the crystalline orientation of the atoms involved. For example, since the GaAs (110) surface does not have a (001) mirror-plane symmetry, there are two distinct ways of forming a complex of interstitial and substitutional Mn. In Fig. 2 the surface Ga atoms are to the right of the surface As atoms to which they are bonded, so that we may consider complexes where the interstitial Mn is to the left or right of the neighboring substitutional dopant; such complexes will be denoted as $i^{\text{As}}(n)s(m)$ and $s(m)i^{\text{As}}(n)$, respectively. Figures 2(c–e) show the configuration of near-surface complexes we have considered in this work. Thus, for example, Fig. 2(c) shows the complexes $s(2)i^{\text{Ga}}(2)$ and $s(2)i^{\text{As}}(2)$, which we discuss below.

Figure 4 shows the calculated total energies of Mn complexes relative to that of the $s(2)i^{\text{As}}(2)$ dopant, which we identify as the lowest-energy configuration. There is a large variation in the energies, up to ~ 1.3 eV above the energy of $s(2)i^{\text{As}}(2)$. We also note that for complexes involving only Mn atoms on the surface [Figs. 4(a) and 4(c)] the lowest-energy configuration occurs when the interstitial site is nearest the substitutional site. Relative to these nearest-neighbor complexes, when interstitial Mn is displaced by lateral translations in the $(\bar{1}10)$ direction, the energy increases dramatically; the next lowest energy configurations are ~ 0.3 eV higher in energy. Thus, diffusion of surface interstitial Mn from high-energy locations (denoted with * and **) to low-energy configurations is likely to form nearest-neighbor complexes on the surface.

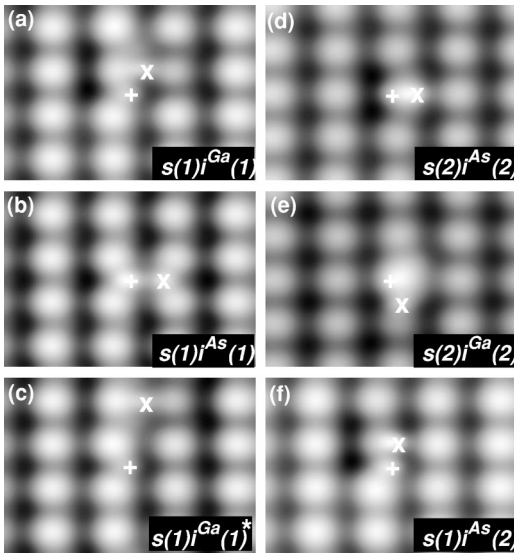


FIG. 5. Simulated STM images for Mn substitutional-interstitial complexes. The locations of substitutional and interstitial Mn are denoted with + and \times , respectively. The crystalline orientation is the same as in Fig. 2.

It is difficult to estimate on energetic grounds alone, the expected number of such complexes. The presence of both the surface and the STM tip create additional complications. For example, the energy of interstitial Mn depends strongly on its proximity to the GaAs (110) surface; an interstitial Mn in the interior of GaAs far from the surface can lower its energy as much as ~ 1 eV by moving to a location just below the surface.³² This suggests that interstitial Mn will diffuse from the bulklike region toward the surface; during the STM scans, these “excess” interstitials will be observed only if they are bound in complexes. Such phenomena are difficult to quantify and beyond the scope of this work. Instead we choose simply to report simulated STM images of several low-energy complexes within the shaded regions of Fig. 4.

B. Simulated STM Images

1. Substitutional-interstitial complexes

Figure 5 shows the simulated images for the low-energy configurations of substitutional-interstitial complexes. The simulated image of the lowest-energy substitutional-interstitial surface complex $s(1)i^{\text{Ga}}(1)$ is shown in Fig. 5(a). There is a reduction in intensity of the As surface atom to the right of the $s(1)$ site and in the region between the As (001) planes to the left of the $s(1)$ site. The simulated images of $s(1)i^{\text{Ga}}(1)^*$ [Fig. 5(c)], $s(2)i^{\text{As}}(2)$ [Fig. 5(d)], and $s(1)i^{\text{As}}(2)$ [Fig. 5(f)] are all similar, but the reduction in the simulated intensity between the As (001) planes to the left of the $s(1)$ site is less apparent. Among these, only the $s(2)i^{\text{As}}(2)$ complex has a $(\bar{1}10)$ mirror-plane symmetry. All four of these simulated images are generally consistent with the characteristics of feature E in the experimental data of Fig. 1. However, since the $s(2)i^{\text{As}}(2)$ complex is much lower in energy (~ 0.5 eV) than the other complexes just described, and since there appears to be only two such fea-

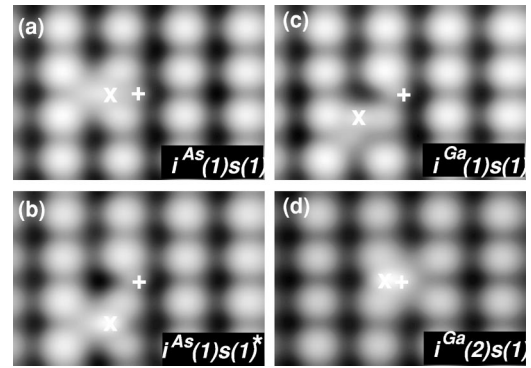


FIG. 6. Simulated STM images for interstitial-substitutional complexes. The locations of substitutional and interstitial Mn are denoted with + and \times , respectively. The crystalline orientation is the same as in Fig. 2.

tures in Fig. 1, we suggest that feature E is most likely a $s(2)i^{\text{As}}(2)$ complex. If this is correct, then the observed apparent displacement of the surface As atom results mainly from an electronic effect rather than a real atomic displacement.

The simulated image of the $s(1)i^{\text{As}}(1)$ complex shown in Fig. 5(b) is rather different than those for the complexes just described. This simulated image obviously has a $(\bar{1}10)$ mirror-plane symmetry and a “butterfly” shape with a region of lower intensity between the Mn atoms. Since there is no (001) mirror plane, the left and right wings of the butterfly are clearly different, with the contribution from the $s(1)$ Mn more intense than that of the $i^{\text{As}}(1)$. Overall, these characteristics are similar to those of feature C, which appears to involve four As surface atoms in neighboring (001) planes. As we discuss below, there are other energetically competitive complexes with similar simulated images, so that we postpone any conclusions regarding feature C until all the relevant complexes have been discussed.

The simulated image of the $s(2)i^{\text{Ga}}(2)$ complex shown in Fig. 5(e) does not have a $(\bar{1}10)$ mirror plane symmetry. In this configuration there is an oblate region of intensity along the As (001) plane and a reduction in the surface As atom intensity nearest the interstitial site. On the basis of the available STM data, we cannot rule out the possibility that some of those features labeled B in Fig. 1 result from $s(2)i^{\text{Ga}}(2)$ complexes.

2. Interstitial-substitutional complexes

Figure 6 shows the simulated images for the low-energy configurations of interstitial-substitutional complexes. The simulated images of the $i^{\text{As}}(1)s(1)$, $i^{\text{As}}(1)s(1)^*$, and $i^{\text{Ga}}(2)s(1)$ complexes are all very similar in shape, with an increase in intensity on the four nearest surface As atoms and between the As (001) planes to the left of the $s(1)$ site for the first two and to the right of the $s(1)$ site for the latter. Obviously, the $i^{\text{As}}(1)s(1)$ and $i^{\text{Ga}}(2)s(1)$ complexes have a $(\bar{1}10)$ mirror-plane symmetry, whereas the $i^{\text{As}}(1)s(1)^*$ appears to approximately have this symmetry. The characteristics of these images are similar to that of the $s(1)i^{\text{As}}(1)$

complex in Fig. 5(b), but with more intensity between the relevant As (001) planes as a result of the interstitial location.

The simulated image of the $i^{\text{Ga}}(1)s(1)$ complex shown in Fig. 6(c) has no apparent symmetry. There is an increase in intensity between the two surface As atoms nearest the $i^{\text{Ga}}(1)$ site, whereas the $s(1)$ Mn is only very weakly visible. Features such as this are not apparent in the experimental data, although XSTM scans of lower doped samples may help clarify whether they are present.

From our STM data and the theoretical simulations, we cannot unambiguously assign feature C to one particular complex among the plausible alternatives: $s(1)i^{\text{As}}(1)$, $i^{\text{As}}(1)s(1)$, $i^{\text{As}}(1)s(1)^*$, $i^{\text{Ga}}(2)s(1)$, $s(1)s(1)$, $s(3)s(3)$, and $s(1)s(3)$. Considering the large number of such features in Fig. 1 and the comparable energies of the different complexes, it is likely that more than one of these dopants are present in the scan area of Fig. 1. Measurements on samples

with much smaller Mn concentration are ongoing and should be able to address these issues in more detail.

VI. SUMMARY

In summary, we have combined first-principles calculations and high-resolution XSTM measurements to characterize Mn-doped GaAs. XSTM on a (110) cleavage plane reveals five reproducible features not found in bulk GaAs. Total-energy calculations were used to screen the most likely configuration of Mn dopants near the GaAs (110) surface. The low-energy configurations were then further scrutinized by comparison of simulated and measured STM images. These comparisons reveal that there are predominantly two types of Mn-related dopants in the sample: (1) those involving only Mn substitutional(s), including both isolated and pairs of substitutionals and (2) complexes composed of substitutional and interstitial Mn.

*Corresponding author. Electronic address: sullivan@dave.nrl.navy.mil

[†]Also at: Nova Research Inc., Alexandria, VA 22308.

¹D. Chiba, K. Takamura, F. Matsukura, and H. Ohno, *Appl. Phys. Lett.* **82**, 3020 (2003).

²K. Ku, S. Potashnik, R. Wang, S. Chun, P. Schiffer, N. Samarth, M. Seong, A. Mascarenhas, E. Johnston-Halperin, R. Myers, A. Gossard, and D. Awschalom, *Appl. Phys. Lett.* **82**, 2302 (2003).

³K. Edmonds, K. Wang, R. Campion, A. Neumann, N. Farley, B. Gallagher, and C. Foxon, *Appl. Phys. Lett.* **81**, 4991 (2002).

⁴T. Dietl, H. Ohno, F. Matsukura, J. Cibert, and D. Ferrand, *Science* **287**, 1019 (2000).

⁵T. Dietl, H. Ohno, and F. Matsukura, *Phys. Rev. B* **63**, 195205 (2001).

⁶S. Sanvito and N. Hill, *J. Magn. Magn. Mater.* **242-245**, 441 (2002).

⁷L. Bergqvist, P.A. Korzhavyi, B. Sanyal, S. Mirbt, I.A. Abrikosov, L. Nordstrom, E.A. Smirnova, P. Mohn, P. Svedlindh, and O. Eriksson, *Phys. Rev. B* **67**, 205201 (2003).

⁸T. Hayashi, Y. Hashimoto, S. Katsumoto, and Y. Iye, *Appl. Phys. Lett.* **78**, 1691 (2001).

⁹S. Potashnik, K. Ku, S. Chun, J. Berry, N. Samarth, and P. Schiffer, *Appl. Phys. Lett.* **79**, 1495 (2001).

¹⁰J. Masek and F. Maca, *Acta Phys. Pol. A* **100**, 319 (2001).

¹¹K.M. Yu, W. Walukiewicz, T. Wojtowicz, I. Kuryliszyn, X. Liu, Y. Sasaki, and J.K. Furdyna, *Phys. Rev. B* **65**, 201303 (2002).

¹²S.C. Erwin and A.G. Petukhov, *Phys. Rev. Lett.* **89**, 227201 (2002).

¹³G. Mahieu, P. Condet, B. Grandidier, J. Nys, G. Allan, D. Stievenard, P. Ebert, H. Shimizu, and M. Tanaka, *Appl. Phys. Lett.* **82**, 712 (2003).

¹⁴B. Grandidier, J. Nys, C. Delerue, D. Stievenard, Y. Higo, and M. Tanaka, *Appl. Phys. Lett.* **77**, 4001 (2000).

¹⁵T. Tsuruoka, R. Tanimoto, N. Tachikawa, S. Ushioda, F. Matsukura, and H. Ohno, *Solid State Commun.* **121**, 79 (2001).

¹⁶T. Tsuruoka, N. Tachikawa, S. Ushioda, F. Matsukura, K. Takamura, and H. Ohno, *Appl. Phys. Lett.* **81**, 2800 (2002).

¹⁷H. Ohno, A. Shen, F. Matsukura, A. Oiwa, A. Endo, S. Katsumoto, and Y. Iye, *Appl. Phys. Lett.* **69**, 363 (1996).

¹⁸B. Noshov, W. Barvosa-Carter, M. Yang, B. Bennett, and L. Whitman, *Surf. Sci.* **465**, 361 (2000).

¹⁹P. Ebert, *Surf. Sci. Rep.* **33**, 121 (1999).

²⁰D. Vanderbilt, *Phys. Rev. B* **41**, 7892 (1990).

²¹G. Kresse and J. Hafner, *J. Phys.: Condens. Matter* **6**, 8245 (1994).

²²G. Kresse and J. Furthmüller, *J. Phys.: Condens. Matter* **6**, 15 (1996).

²³G. Kresse and J. Hafner, *Phys. Rev. B* **47**, 558 (1993).

²⁴G. Kresse and J. Furthmüller, *Phys. Rev. B* **54**, 11 169 (1996).

²⁵J. Tersoff and D.R. Hamann, *Phys. Rev. Lett.* **50**, 1998 (1983).

²⁶M. van Schilfgarde and O.N. Mryasov, *Phys. Rev. B* **63**, 233205 (2001).

²⁷G. Alvarez, M. Mayr, and E. Dagotto, *Phys. Rev. Lett.* **89**, 277202 (2002).

²⁸G. Alvarez and E. Dagotto, cond-mat/0303350 (unpublished).

²⁹J. Blinowski and P. Kacman, *Phys. Rev. B* **67**, 121204 (2003).

³⁰P. Mahadevan and A. Zunger, *Phys. Rev. B* **68**, 075202 (2003).

³¹C. Timm, F. Schafer, and F. von Oppen, *Phys. Rev. Lett.* **89**, 137201 (2002).

³²J.M. Sullivan and S. C. Erwin (unpublished).